# Structure of the scalar mesons $f_0(980)$ and $a_0(980)$

G. Janssen*
*Department of Physics, State University of New York at Stony Brook, Stony Brook, New York 11794*

B. C. Pearce
*Department of Physics and Mathematical Physics, University of Adelaide, Adelaide, S.A. 5005, Australia*

K. Holinde and J. Speth
*Institut für Kernphysik, Forschungszentrum Jülich GmbH, D-52425 Jülich, Germany*
(Received 22 November 1994)

We investigate the structure of the scalar mesons $f_0(980)$ and $a_0(980)$ within realistic meson-exchange models of the $\pi\pi$ and $\pi\eta$ interactions. Starting from a modified version of the Jülich model for $\pi\pi$ scattering we perform an analysis of the pole structure of the resulting scattering amplitude and find, in contrast with existing models, a somewhat large mass for the $f_0(980)$ ($m_{f_0} = 1015$ MeV, $\Gamma_{f_0} = 30$ MeV). It is shown that our model provides a description of $J/\psi \to \phi\pi\pi/\phi KK$ data comparable in quality with those of alternative models. Furthermore, the formalism developed for the $\pi\pi$ system is consistently extended to the $\pi\eta$ interaction leading to a description of the $a_0(980)$ as a dynamically generated threshold effect (which is therefore neither a conventional $q\bar{q}$ state nor a $K\bar{K}$ bound state). Exploring the corresponding pole position the $a_0(980)$ is found to be rather broad ($m_{a_0} = 991$ MeV, $\Gamma_{a_0} = 202$ MeV). The experimentally observed smaller width results from the influence of the nearby $K\bar{K}$ threshold on this pole.

PACS number(s): 14.40.Cs, 11.80.Gw, 13.25.Gv, 13.75.Lb

## I. INTRODUCTION

With increasing experimental information about the different members of the meson spectrum it becomes more and more important to develop a consistent understanding of the observed mesons from a theoretical point of view. For the low-lying pseudoscalar, vector, and tensor mesons this has been done quite successfully within the framework of the simple quark model assuming the mesons to be quark-antiquark ($q\bar{q}$) states grouped together into nonets. For the scalar mesons, however, several questions still remain to be answered, most of them related to the nature of the experimentally observed mesons $f_0(980)$ and $a_0(980)$.

In a long-standing controversial discussion the $f_0(980)$ has been described as, for example, a conventional $q\bar{q}$ meson [1], a $K\bar{K}$ molecule [2], or a multiquark state [3]. In order to discriminate between different models Morgan and Pennington [4,5] recently investigated new data on the decay $J/\psi \to \phi\pi\pi/\phi KK$ [6,7], concluding that a conventional Breit-Wigner (i.e., $q\bar{q}$) structure is most probable for the $f_0(980)$. They claim that the $\pi\pi/K\bar{K}$ amplitude is characterized by two poles near the $K\bar{K}$ threshold on the $[bt]$ (second) and $[bb]$ (third) sheet (see Ref. [8] and Sec. II for sheet structure and notation). In the Jülich model of the $\pi\pi$ interaction [9] the $f_0(980)$ appears to be a pure $K\bar{K}$ bound state generated dynamically by vector-meson exchange. Such a state has only one nearby pole on the $[bt]$ sheet, a structure seemingly disfavored by the results of Ref. [4]. However, it has been pointed out by Zou and Bugg [10] that a model with only one nearby $[bt]$ sheet pole (similar to a $K\bar{K}$ bound state) but a very broad $[bb]$ sheet pole is also compatible with the $J/\psi$ data and this conclusion was very recently confirmed by Morgan and Pennington [11]. Though $J/\psi$ decay thus may no longer be regarded as the crucial discriminant for the structure of the $f_0(980)$ it remains an important source of experimental information. We have therefore fitted this data with the $\pi\pi/K\bar{K}$ amplitude resulting from our meson-exchange model and obtained a reasonable description which is comparable in quality with those of the alternative models discussed above.

What turns out to be quite different in our analysis is the rather large mass (interpreted as the pole position) of the $f_0(980)$ ($m_{f_0} = 1.015$ GeV; see Sec. III) which is a consequence of its $K\bar{K}$ bound state nature in combination with a rather strong coupling between $\pi\pi$ and $K\bar{K}$ channels. While there has been considerable discussion in the literature concerning the width of the $f_0(980)$ [5,10,12], there seems to be a consensus that the mass lies between 0.97 and 1.0 GeV. Interestingly, our value for the mass is somewhat larger than this due to the strong influence of the $K\bar{K}$ threshold.

Closely related to the $f_0(980)$ is the $a_0(980)$ which is observed in the $\pi\eta$ channel. Both mesons couple to the $K\bar{K}$ channel and their masses lie very close to the $K\bar{K}$ threshold. As with the $f_0(980)$, the nature of the $a_0(980)$ is still under discussion, especially since the available

*Present address: Institut für Kernphysik, Forschungszentrum Jülich, D-52425 Jülich, Germany.

 

experimental information about $\pi\eta$ scattering is rather poor compared to $\pi\pi$ scattering [13]. In Ref. [2] the $f_0(980)$ and $a_0(980)$ emerge from a nonrelativistic quark model calculation to be degenerate $K\overline{K}$ bound states. However, while the Jülich model of the $\pi\pi$ interaction comes to the same conclusion for the $f_0(980)$ the situation turns out to be rather different for the $a_0(980)$. The $K\overline{K}$ interaction generated by vector-meson exchange, which for isospin $I = 0$ is strong enough to generate a bound state, is much weaker for $I = 1$, making a degeneracy of $a_0(980)$ and $f_0(980)$ impossible.

It is therefore one aim of this paper to address the question of whether the close relation between $a_0(980)$ and $f_0(980)$ expressed by their similar properties (masses, proximity to $K\overline{K}$ threshold, etc.) can be understood in the framework of our meson-exchange model. By extending the $\pi\pi$ model consistently to the $\pi\eta$ system we find that this is indeed possible. We obtain a model where both the $a_0(980)$ and $f_0(980)$ originate from the coupling to the $K\overline{K}$ channel. However, the underlying structure turns out to be quite different. In contrast with the $f_0(980)$, the $a_0(980)$ would not appear to be a $K\overline{K}$ bound state but a dynamically generated threshold effect with a relatively broad pole on the $[bt]$ sheet. We find poles responsible for the observed $a_0(980)$ and $f_0(980)$ at complex energies $(\mathrm{Re}E, \mathrm{Im}E) = (991, \pm 101)$ MeV and $(1015, \pm 15)$ MeV, respectively. Despite such different pole positions, the observed position and width of the structure in the cross sections turn out to be rather similar. This is directly attributable to the proximity of the $K\overline{K}$ threshold at 991 MeV.

Section II contains the basic ingredients of our model for $\pi\pi$ and $\pi\eta$ scattering as well as the underlying formalism relevant for the investigation of the $f_0(980)$ and $a_0(980)$. Results are presented and discussed in Sec. III. The paper ends with concluding remarks in Sec. IV.

## II. MODEL

In order to understand the underlying structure of the scalar mesons $f_0(980)$ and $a_0(980)$ (referred to as $f_0$ and $a_0$ in the following) we have to develop realistic models for $\pi\pi$ and $\pi\eta$ scattering respectively. The basis for the present work is the Jülich meson exchange model for the $\pi\pi$ interaction whose evaluation has been discussed in detail in former work [9,14]. Compared to the original version some modifications have been performed which will be discussed in the following.

The potentials for $\pi\pi \to \pi\pi$, $\pi\pi \to K\overline{K}$, and $K\overline{K} \to K\overline{K}$ are generated from the diagrams shown in Fig. 1. The figure shows only $s$- and $t$-channel diagrams; $u$-channel processes corresponding to the included $t$-channel processes are also included when they contribute. The scalar-isoscalar particle denoted by $\epsilon$ in Fig. 1 effectively includes the singlet and the octet member of the scalar nonet. We investigated the effects of $t$-channel $f_2(1270)$ and $\epsilon$ exchange but found their effects to be negligible. Hence, the results presented here do not include them. For completeness we have also added the $s$-channel pole diagrams $\pi\pi/K\overline{K} \to \epsilon, \rho, f_2 \to \pi\pi/K\overline{K}$,

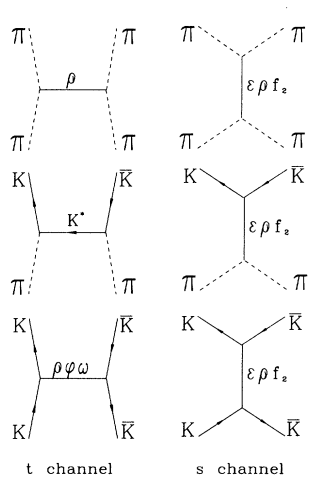


FIG. 1. Diagrams included in the potentials $\pi\pi \to \pi\pi$, $\pi\pi \to K\overline{K}$, and $K\overline{K} \to K\overline{K}$.

which enable a unified description of all partial waves. However, the $s$-channel $\rho$ and $f_2$ poles do not contribute to the description of the $f_0(980)$ or $a_0(980)$.

The coupling constant $g_{\rho\pi\pi}$, required for $t$- and $u$-channel exchange diagrams, is determined from the decay widths of the $\rho$ (Table I). The $s$-channel $\epsilon$, $\rho$, and $f_2$ exchanges are renormalized by solving Eq. (1) below, and so the bare couplings and bare masses are adjusted to reproduce experimental data in the appropriate partial waves (see Tables II and III). All remaining coupling constants are determined from SU(3) symmetry relations, and standard assumptions about the octet-singlet mixing angles, as demonstrated in Ref. [9] (see Tables I and II).

The scattering amplitudes are obtained by iterating these potentials by using a coupled-channel scattering equation. We follow the approach of [14] and use the Blankenbecler-Sugar (BS) formalism [15] rather than time-ordered perturbation theory [9]. The partial wave decomposed, coupled-channel scattering amplitude $T_{ij}$ $[i, j = \pi\pi(\pi\eta), K\overline{K}$; indices for total angular momentum and isospin are suppressed] is therefore given by

$$T_{ij}(k', k; E) = V_{ij}(k', k; E) + \sum_l \int dk'' k''^2 V_{il}(k', k''; E) \times G_l(k''; E) T_{lj}(k'', k; E), \quad (1)$$

TABLE I. Vertex parameters for $t$ channel exchanges. Relations between coupling constants are obtained using SU(3) and ideal mixing between the octet and singlet.

| Vertex | $g$ | $\Lambda$ [MeV] |
|---|---|---|
| $\pi\pi\rho$ | 6.04 | 1355 |
| $\pi KK^*$ | $g_{\pi KK^*} = g_{\pi\overline{KK}^*} = -\frac{1}{2} g_{\pi\pi\rho}$ | 1900 |
| $KK\rho$ | $g_{KK\rho} = g_{\overline{KK}\rho} = \frac{1}{2} g_{\pi\pi\rho}$ | 1850 |
| $KK\omega$ | $g_{KK\omega} = -g_{\overline{KK}\omega} = \frac{1}{2} g_{\pi\pi\rho}$ | 2800 |
| $KK\phi$ | $g_{KK\phi} = -g_{\overline{KK}\phi} = \frac{1}{\sqrt{2}} g_{\pi\pi\rho}$ | 2800 |
| $\eta KK^*$ | $g_{\eta KK^*} = -g_{\eta\overline{KK}^*} = -\frac{\sqrt{3}}{2} g_{\pi\pi\rho}$ | 3290 |

TABLE II. Vertex parameters for $s$-channel exchanges. The exchanged meson is identified with a superscript (0) since it is a bare meson. The $\epsilon^{(0)}$ contributes to the description of the $f_0(980)$. None of the other parameters contribute to $f_0$ or $a_0$.

| Vertex | $g$ | $\Lambda$ [MeV] |
|---|---|---|
| $\pi\pi\epsilon^{(0)}$ | 0.286 | 925 |
| $KK\epsilon^{(0)}$ | $-0.286$[a] | 1200 |
| $\pi\pi\rho^{(0)}$ | 5.32 | 1647 |
| $KK\rho^{(0)}$ | $\frac{1}{2}g_{\pi\pi\rho^{(0)}}$ | 830 |
| $\pi\pi f_2^{(0)}$ | 1.23 | 995 |
| $KKf_2^{(0)}$ | $\frac{2}{3}g_{\pi\pi f_2^{(0)}}$ | 937 |

[a]Since the singlet-octet mixing angle for the scalar nonet is not known, $g_{KK\epsilon^{(0)}}$ is a free parameter.

where $E=\sqrt{s}$ denotes the total center of mass energy.

The BS two-meson propagator for channel $l$ is denoted $G_l(k'';E)$ and can be written as

$$G_l(k'';E)=\frac{\omega_1+\omega_2}{(2\pi)^3 2\omega_1\omega_2}\frac{1}{E^2-(\omega_1+\omega_2)^2}\ , \qquad (2)$$

where $\omega_1$ and $\omega_2$ are the on-mass shell energies for particle 1 and 2, respectively, $\omega_\alpha=\sqrt{k''^2+m_\alpha}$. The on-shell momentum $k_0$ for channel $l$ is defined by the singularity of $G_l$ to be

$$k_0=\frac{\sqrt{[E^2-(m_1+m_2)^2][E^2-(m_1-m_2)^2]}}{2E}\ . \qquad (3)$$

In order to determine the correct values for the mass and width of the $f_0$ as they are predicted by our model, it is necessary to explore the position of the poles of the scattering amplitude $T$. This can only be done by taking into account the sheet structure of the scattering amplitude which is imposed by the existence of $\pi\pi$ and $K\overline{K}$ thresholds. We will use the notation of [8] for referring to the various sheets using a two character string composed of the letters $t$ and $b$ to signify on which sheet of each threshold the energy lies. The conventional second sheet, for example, is therefore denoted by $[bt]$ indicating that the energy is on the bottom sheet of the $\pi\pi$ channel and the top sheet of the $K\overline{K}$ channel. The sheet definition is visualized in Fig. 2.

To determine the poles of the scattering amplitude $T_{ij}$ generated by Eq. (1) we solve the eigenvalue equation [16]

$$\sum_l[\lambda(E)\delta_{il}-V_{il}(E)G_l(E)]\phi_l(E)\equiv\sum_l I_l(E)=0, \qquad (4)$$

where $\phi_l(E)$ denotes the eigenfunction for channel $l$, and search for complex energies $E_R$ that result in an eigenvalue $\lambda(E_R)=1$.

TABLE III. Bare masses $M_0$ used in the $s$-channel exchanges, in MeV.

| $\epsilon^{(0)}$ | $\rho^{(0)}$ | $f_2^{(0)}$ |
|---|---|---|
| 1520 | 1125 | 1660 |

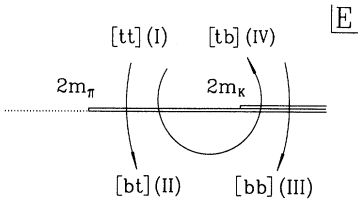


FIG. 2. Sheets of the energy plane and their labeling. In parentheses we have given the conventional notation. The double lines symbolize $\pi\pi$ and $K\overline{K}$ unitarity cuts.

When the integral appearing in the momentum representation of Eq. (4) is performed, care must be taken to avoid the poles of $G_l$ and to take into account the multisheet structure of $T_{ij}$. Following the approach of Ref. [8] this can be done for physical (i.e., on the top sheet) energies $E_t$ simply by rotating the contour of integration into the complex plane. For energies $E_b$ on the bottom sheet of threshold $l$ the residue of the pole of $G_l(k'';E)$ at $k''=-k_0$ must be included. In summary we obtain [8]

$$I_l(E_t)=\int_C dk''k''^2\left[\lambda(E_t)\delta(k-k'')\delta_{il} -V_{il}(k,k'';E_t)G_l(k'';E_t)\right]\phi_l(k'';E_t) \qquad (5)$$

and

$$I_l(E_b)=\int_C dk''k''^2\left[\lambda(E_b)\delta(k-k'')\delta_{il} -V_{il}(k,k'';E_b)G_l(k'';E_b)\right]\phi_l(k'';E_b) -2\pi i\frac{(-k_0)}{4(2\pi)^3E_b}V_{il}(k,-k_0;E_b)\phi_l(-k_0;E_b)\ , \qquad (6)$$

where the contour $C$ is as shown in Fig. 3(a) for $\mathrm{Im}(E)\geq 0$ and as in Fig. 3(b) for $\mathrm{Im}(E)<0$.

In practice, we implement this by using a Gaussian quadrature rule to reduce Eqs. (4)–(6) to a matrix eigenvalue equation, and then set $\lambda=1$ and search for energies such that

$$\det[1-V(E)G(E)]=0. \qquad (7)$$

In solving Eq. (4), problems may arise from the $t$- and $u$-channel contributions to the potential $V_{il}$. Inserting the off-shell prescription of the BS formalism (see the Appendix) we obtain, for the $t$-channel diagrams (and analogously for the $u$-channel diagrams),

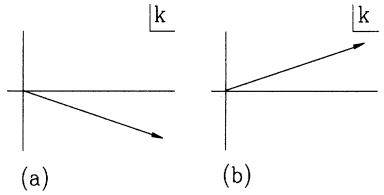


FIG. 3. Rotated integration contours used for evaluating the integrals of Eqs. (5) and (6).

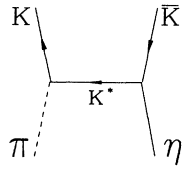


FIG. 4. Diagram included in the potential $\pi\eta \to K\overline{K}$.

$$V_{il}(k',k;E) \propto [t-M^2]^{-1} = [-k^2-k'^2+2kk'\cos\theta - M^2]^{-1}\ , \quad (8)$$

where $M$ denotes the mass of the exchanged particle and $\theta$ is the scattering angle. For a fully off-shell potential this propagator never becomes singular since $k$ and $k'$ vary along the same rotated contour. This is not true, however, for the half off-shell potentials appearing in Eq. (6) which leads to a restriction on the energy region that can be searched using this method. We have calculated the locations of all these singularities in the complex energy plane and found them to be far away from the energy region of interest to this investigation. This is also true for the $\pi\eta$ channel where the equivalent of Eq. (8) looks more complicated due to the unequal masses.

The formalism for calculating the $J/\psi \to \phi\pi\pi/\phi KK$ mass spectra has been described in detail in Refs. [4,5,10]. The input is the $\pi\pi/K\overline{K}$ amplitudes $T_{ij}$ which in our model are generated by Eq. (1). Our amplitudes are normalized differently to those of Ref. [10], with the relation between the two being given by

$$T_{ij}^{[10]} = [64\pi^2]^{-1} T_{ij}. \quad (9)$$

Since the difference is just a constant factor it is absorbed in the overall normalization of the $J/\psi$ mass spectra. The amplitudes for $J/\psi$ decay are given by

$$F(\psi \to \phi\pi^+\pi^-) = \left[\tfrac{2}{3}\right]^{1/2}[\alpha_1(s)T_{11} + \alpha_2(s)T_{21}],$$
$$F(\psi \to \phi K^+K^-) = \left[\tfrac{1}{2}\right]^{1/2}[\alpha_1(s)T_{12} + \alpha_2(s)T_{22}], \quad (10)$$

with the real coupling functions $\alpha_i$ parametrized by

$$\alpha_i(s) = \gamma_{i0} + \gamma_{i1}s\ , \quad (11)$$

where $\gamma_{i0}$ and $\gamma_{i1}$ are free parameters. The experimentally observed mass spectra are then formed from the modulus squared of these amplitudes multiplied by phase space and an overall normalization factor.

Finally, we develop our formalism for the $\pi\eta$ interaction in order to obtain an understanding of the $a_0$ meson. As for the $f_0$, we include the coupling to the $K\overline{K}$ channel, where the corresponding direct $K\overline{K}$ interaction is taken to be exactly the same as for the $\pi\pi$ case, projected now onto isospin $I = 1$. In addition, our model includes the $t$-channel $K^*$ exchange diagram shown in Fig. 4 (and corresponding $u$-channel diagram) which couples the $\pi\eta$ channel to $K\overline{K}$. The spin-momentum structure of this potential is given by the same general expression for the

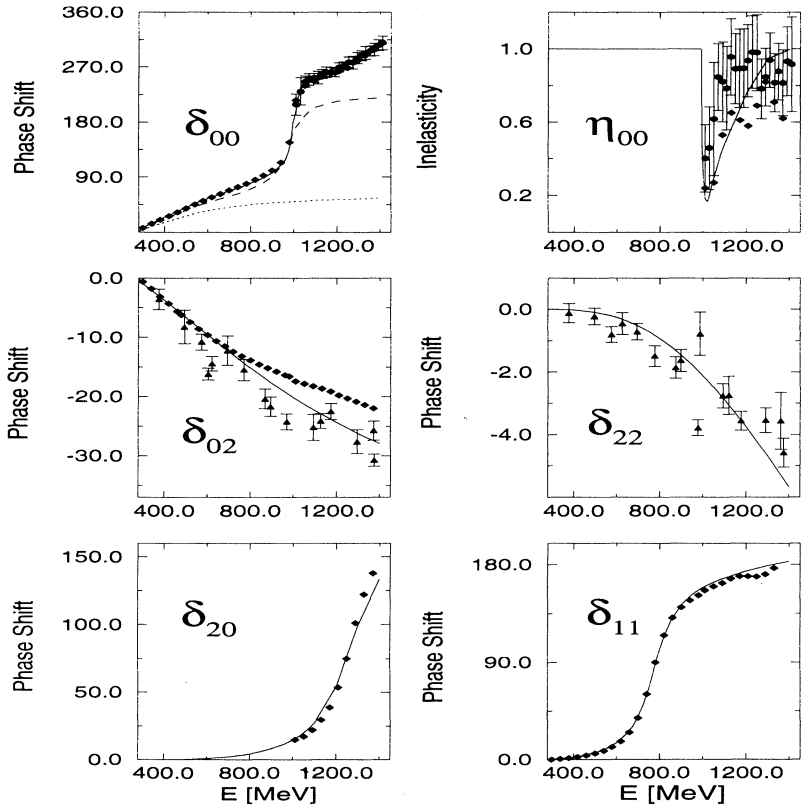


FIG. 5. Results of the modified Jülich $\pi\pi$ interaction model for elastic $\pi\pi$ scattering. Data are from Refs. [20,26,27]. The solid line shows the result of our full model. For the dashed line in $\delta_{00}$ we have excluded the $\epsilon$ $s$-channel pole diagram. The dotted line contains only $t$- and $u$-channel $\rho$ exchange.

interaction between two pseudoscalar particles which has been derived for the $\pi\pi$ interaction (see Ref. [9] and the Appendix). The potential corresponding to Fig. 4 is obtained by using the appropriate coupling constants and isospin factors (Tables I and IV) and the BS off-shell prescription for different-mass particles (Appendix).

Since the coupling constant $g_{\eta KK^*}$ is related by SU(3) symmetry to $g_{\rho\pi\pi}$, the entire $\pi\eta$ $T$ matrix is obtained with the addition of only one new parameter, the cutoff mass $\Lambda_{\eta KK^*}$.

The $\pi\eta$ scattering amplitude $T$ and the location of its poles follow from exactly the same formalism as was developed for the $\pi\pi$ interaction. Since the $\epsilon$ and $f_2$ $t$-channel exchanges were found to be negligible, this model does not include any direct $\pi\eta \to \pi\eta$ potential.

## III. RESULTS AND DISCUSSION

Having specified all of the relevant formalism, we first look at elastic $\pi\pi$ scattering where we essentially reproduce the results of Ref. [9] within our modified model. Figure 5 shows the result of our fit to experimental data on elastic $\pi\pi$ scattering for the $JI = 00$ ($f_0$) partial wave as well as for $JI = 02$, 11, 20, and 22 with the complete set of parameters given in Tables I–III. As could be expected from Refs. [9,14] we obtain quite good overall agreement with the experimental situation. The quality of the total fit obtained with a relatively small number of parameters demonstrates the validity of the model. In particular we note that $t$-channel $\rho$ exchange is the sole contributor to $JI = 02$ and 22, and, as can be seen in the dotted curve in Fig. 5, provides a substantial part of the low energy $JI = 00$ interaction. This suggests that the spin-isospin structure provided by the $t$-channel meson exchanges arising from a Lagrangian with effective meson degrees of freedom is substantively correct.

In particular we are able to describe the structure appearing around 1.0 GeV in the isoscalar $\pi\pi$ $S$ wave which is assigned to the $f_0$ meson. In our model this resonance like behavior is generated dynamically by the strong attraction arising from $\rho$, $\omega$, and $\phi$ exchange in the $K\overline{K}$ channel and we therefore do *not* need a genuine scalar resonance with mass around 1.0 GeV. This is demonstrated for $\delta_{00}$ by the dashed line in Fig. 5 where we have excluded the $s$-channel $\epsilon$ pole diagram. On the other hand, it is definitely necessary to include a heavy scalar particle, namely, the $\epsilon$ with mass around 1.4 GeV, to describe the experimental data beyond 1.0 GeV (see the solid line in Fig. 5). This particle may be interpreted as the member of the scalar nonet; i.e., it effectively parametrizes the effect of both the isoscalar singlet and octet contributions and any other higher mass states present in the scalar-isoscalar spectrum. For smaller energies ($E \simeq 0.5$ GeV) the $\pi\pi$ $S$ wave is characterized by a sizable phase shift dominantly generated by $t$-channel $\rho$ exchange. The corresponding attraction between the two pions forms a broad background to the $f_0$ (dotted curve in Fig. 5).

In order to be able to investigate the structure of the $f_0$ meson the reliability of our model in the $JI = 00$ partial wave close to $K\overline{K}$ threshold should be checked in more detail. Figure 6 shows the comparison of our calculation with experimental data on the $\pi\pi \to K\overline{K}$ channel. The figure shows data obtained from three different direct measurements of $\pi\pi \to K\overline{K}$ cross sections [17–19] together with results inferred from elastic $\pi\pi \to \pi\pi$ scattering [20] which we deduced by assuming that the inelasticity of the $\pi\pi$ amplitude is entirely due to $K\overline{K}$ production. As can be seen from the figure, the $K\overline{K}$ production cross sections are rather poorly known experimentally. Our calculation agrees reasonably well with the most recent data of Ref. [17] (shown using open circles in Fig. 6).

The fact the $\pi\pi/K\overline{K}$ amplitude is underconstrained by the available data on meson-meson scattering has already been discussed by Morgan and Pennington (see Fig. 4 of Ref. [4] which corresponds to our Fig. 6). In order to extend the set of experimental data and to be able to decide about the structure of the $f_0$ they have investigated the role of the decay $J/\psi \to \phi\pi\pi/\phi K\overline{K}$. Though a recent discussion [5,10,11] has shown that this data does not enable one to make a definitive statement about the nature of the $f_0$, the $J/\psi$ decay remains a very valuable addition to an analysis of the $\pi\pi/K\overline{K}$ scattering amplitude. We have therefore calculated the corresponding mass distributions using the scattering amplitude obtained from our meson-exchange model and compared them with experimental data.

Figure 7 shows the result of our fit to the $J/\psi$ decay data from DM2 [6] and MK3 [7]. The fit was obtained using $\{\gamma_{10}, \gamma_{11}, \gamma_{20}, \gamma_{21}\} = \{7.716, -16.399, 24.670, -9.418\}$ [see Eq. (11)] ($\gamma_{10}$ and $\gamma_{20}$ are dimensionless while $\gamma_{11}$ and $\gamma_{21}$ are in GeV$^{-2}$). The fit demonstrates that our model is able to reproduce this data quite well. Moreover, the quality of the fit is comparable in quality with those of alternative models [5,10], leading to the conclusion that the bound state structure of the $f_0$ is not disfavored by the $J/\psi$ criterion.

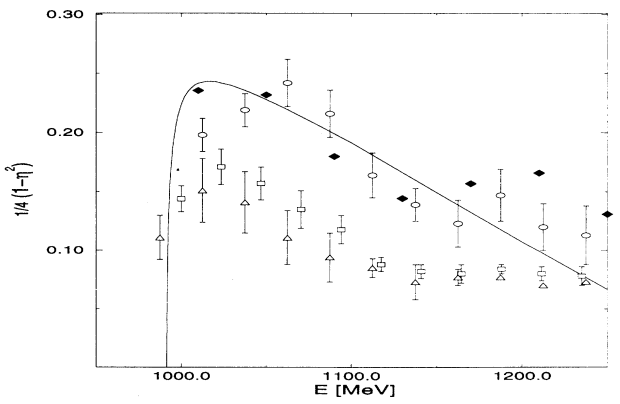


FIG. 6. Results of the modified Jülich $\pi\pi$ interaction model compared with data on the $\pi\pi \to K\overline{K}$ channel in terms of $\frac{1}{4}(1-\eta^2)$. Data are from Refs. [17] (open circles), [18] (open triangles), [19] (open squares), and [20] (solid diamonds, from inelasticity of elastic $\pi\pi$ amplitude).

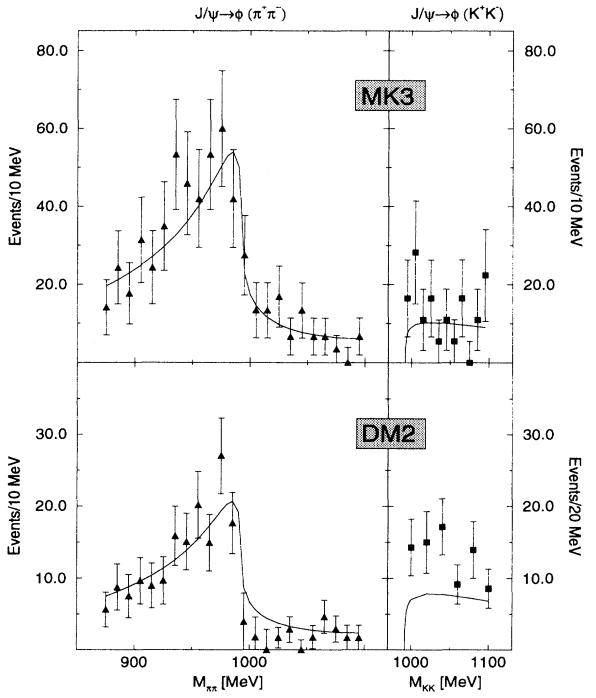


FIG. 7. Fit to $J/\psi \to \phi\pi\pi/\phi KK$ data. The upper panel shows the fit to data of Ref. [7] and the lower panel to Ref. [6].

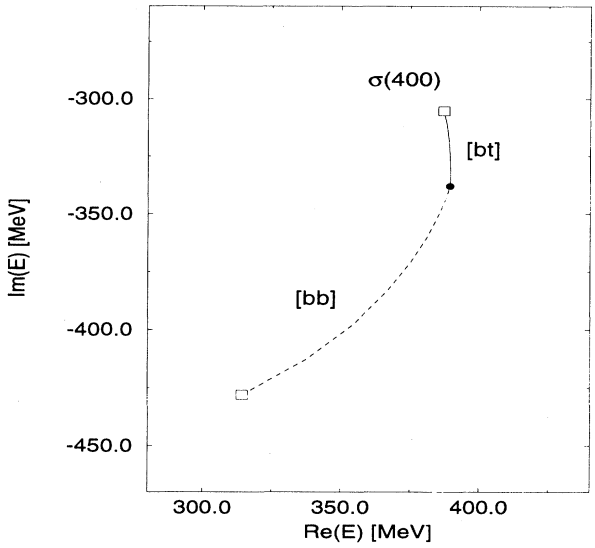


FIG. 8. The positions of the $\sigma(400)$ pole on $[bt]$ and its shadow pole on $[bb]$ for our full model (squares). For decreasing $\pi\pi/K\overline{K}$ coupling they move along the curves indicated and the dot gives their position in the zero coupling limit.

Having obtained a model which is compatible with the available experimental data sets, we are now in a position to discuss the pole positions of the scattering amplitude in the isoscalar $\pi\pi$ $S$ wave.

Looking at smaller energies first, we find a very broad pole on the $[bt]$ sheet at complex energy $(\mathrm{Re}E, \mathrm{Im}E) = (387, \pm 305)$ MeV and its shadow-pole counterpart [8] on the $[bb]$ sheet at $(314, \pm 428)$ MeV (see Table V). At vanishing $\pi\pi/K\overline{K}$ coupling this pole is found on both $K\overline{K}$ sheets at the same position but when the coupling is increased they move apart. This is demonstrated in Fig. 8 where we turned off the $\pi\pi/K\overline{K}$ coupling gradually, thus proving that we have really found a pole and its corresponding shadow pole. This shows that these poles are generated by the strong $t$-channel $\rho$ exchange in the $\pi\pi \to \pi\pi$ potential. The pole closest to the physical region, namely the one on $[bt]$, is the origin of the large $\pi\pi$ $S$ wave phase shifts below 1.0 GeV (see $\delta_{00}$ in Fig. 5). Following Ref. [10] we denote it $\sigma(400)$.

We find an additional pair of connected poles at lower energies [$\mathrm{Re}(E) \simeq 500$ MeV] on sheets $[tb]$ and $[bb]$, indicating that this time the origin is the direct $K\overline{K}$ interaction. However, since both $[tb]$ and $[bb]$ poles are far away from the physical region they do not have any effect on physical observables and are therefore quite unimportant for the present investigation.

Looking at higher energies, we find the poles generated by the $\epsilon$ $s$-channel diagram necessary to describe data above 1.0 GeV. Including exclusively this diagram and turning off the $\pi\pi/K\overline{K}$ coupling a pole is found at $(1354, \pm 167)$ MeV on $[bt]$ and $[bb]$ sheets (Fig. 9, point $A$). The $t$-channel contributions to the $\pi\pi$ potential shift both poles to point $B$ of Fig. 9 before they move apart when the $\pi\pi/K\overline{K}$ coupling is increased. Whereas the physically unimportant $[bt]$ pole moves to very high energies the $[bb]$ pole is finally found at $(1346, \pm 249)$ MeV (see Table V). This pole, lying closest to the physical region, defines the parameters of the genuine scalar particle which effectively includes the singlet and the octet member of the scalar nonet. We denote it by $f_0(1400)$ although it is more likely an effective parametrization

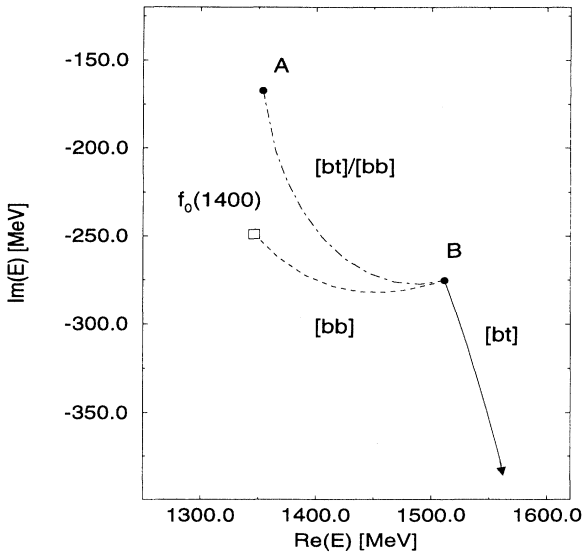


FIG. 9. The $f_0(1400)$ pole on $[bb]$ and its shadow pole on $[bt]$. The notation is as in Fig. 8. For point $A$, only the diagram $\pi\pi \to \epsilon \to \pi\pi$ is considered while point $B$ includes in addition the $t$-channel diagrams for $\pi\pi \to \pi\pi$.

of two scalar resonances, such as $f_0(1400)$ and $f_0(1590)$. Both poles, $\sigma(400)$ and $f_0(1400)$ form a background to the $f_0(980)$. A similar structure has been observed in Ref. [12].

Next we investigate the energy region around the $K\overline{K}$ threshold and find a single pole on the $[bt]$ sheet at $(1015, \pm 15)$ MeV which clearly has to be assigned to the $f_0$ meson and to the corresponding structure in $\pi\pi$ phase shifts and inelasticities. We therefore obtain

$$m_{f_0} = 1015 \text{ MeV}, \qquad \Gamma_{f_0} = 30 \text{ MeV}. \tag{12}$$

In the zero $\pi\pi/K\overline{K}$ coupling limit the pole moves back to $(985, 0)$ MeV (i.e., on the real axis and below the $K\overline{K}$ threshold) and appears on sheets $[tt]$ and $[bt]$ (see Fig. 10). This demonstrates the bound state nature of the $f_0$ within our model.

Compared to other models [4,12] we find a rather high mass (when interpreted as the pole position) for the $f_0$. This is a consequence of the relatively strong coupling between the $\pi\pi$ and $K\overline{K}$ channels which moves the pole from the real axis to its final position. A similar movement of a bound state pole to energies above the corresponding threshold was already found in Ref. [8], and as the strength of the $\pi\pi/K\overline{K}$ coupling is constrained by the fit to experimental data, the relatively high mass seems to be a more general feature of our bound state model for the $f_0$.

The fact that the pole is on the $[bt]$ sheet and above the $K\overline{K}$ threshold means that its effect will be seen most strongly at the threshold. This can be seen in, for example, the partial wave cross section which is shown in Fig. 11. The most evident feature is the strong dip in the cross section which occurs precisely at the $K\overline{K}$ threshold. There is no structure evident near the pole at $(1015, \pm 15)$ MeV. Clearly it is insufficient to simply quote the mass parameters of the $f_0(980)$ without describing in detail how the threshold is incorporated since the two are inextricably linked.

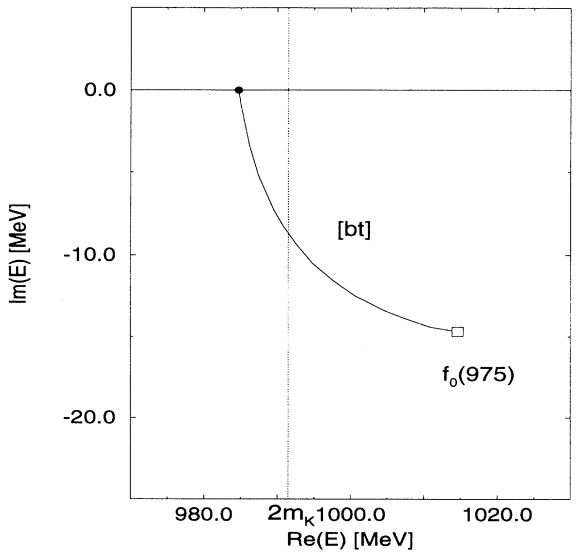


FIG. 10. The $f_0(980)$ pole on $[bt]$. Notation as in Fig. 8.

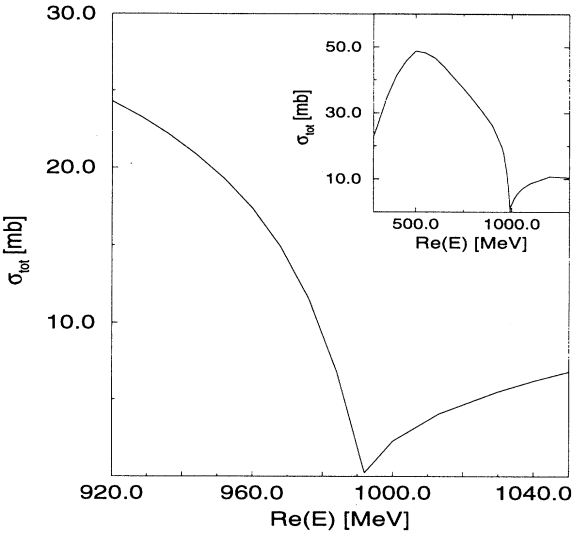


FIG. 11. The calculated $JI = 00$ $\pi\pi$ cross section.

For completeness, we finally look at the $\rho$ ($JI = 11$) channel. As could be expected we observe a pole on the $[bt]$ sheet and an unimportant shadow pole on the $[bb]$ sheet with the position of the former found at $(775, \pm 82)$ MeV. The deviation from the usually given Breit-Wigner parameters ($m_\rho = 768.1$ MeV, $\Gamma_\rho/2 = 76$ MeV) is due to the existence of a nonpole background generated by the $t$-channel diagrams.

Next we turn our attention to the $\pi\eta$ channel and the structure of the $a_0$. It was already pointed out that we want to extend the concepts applied to the $\pi\pi$ interaction *consistently* to the $\pi\eta$ system; therefore, the $K\overline{K}$ interaction required for a $\pi\eta/K\overline{K}$ coupled-channel approach

TABLE IV. Isospin factors for each meson exchange diagram used.

| Potential | Meson | Type | Factor $f$ | | |
|---|---|---|---|---|---|
| | | | $I=0$ | $I=1$ | $I=2$ |
| $\pi\pi \to \pi\pi$ | $\rho$ | $t$ channel | $-2$ | $-1$ | 1 |
| | $\epsilon^{(0)}$ | $s$ channel | 3 | 0 | 0 |
| | $\rho^{(0)}$ | $s$ channel | 0 | 2 | 0 |
| | $f_2^{(0)}$ | $s$ channel | 3 | 0 | 0 |
| $\pi\pi \to K\overline{K}$ | $K^*$ | $t$ channel | $\sqrt{6}$ | 2 | — |
| | $\epsilon^{(0)}$ | $s$ channel | $-\sqrt{6}$ | 0 | — |
| | $\rho^{(0)}$ | $s$ channel | 0 | 2 | — |
| | $f_2^{(0)}$ | $s$ channel | $-\sqrt{6}$ | 0 | — |
| $K\overline{K} \to K\overline{K}$ | $\rho$ | $t$ channel | $-3$ | 1 | — |
| | $\omega$ | $t$ channel | 1 | 1 | — |
| | $\phi$ | $t$ channel | 1 | 1 | — |
| | $\epsilon^{(0)}$ | $s$ channel | 2 | 0 | — |
| | $\rho^{(0)}$ | $s$ channel | 0 | 2 | — |
| | $f_2^{(0)}$ | $s$ channel | 2 | 0 | — |
| $\pi\eta \to K\overline{K}$ | $K^*$ | $t$ channel | — | $\sqrt{2}$ | — |

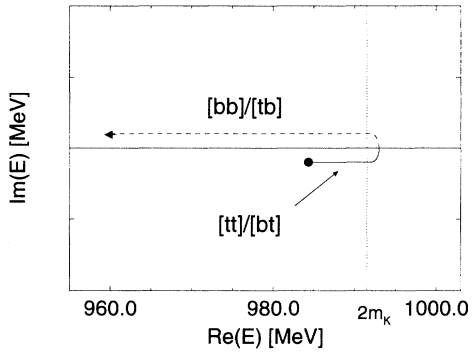


FIG. 12. The movement of the $K\overline{K}$ bound-state pole as the strength of $\rho$ exchange decreases (finally becoming repulsive). Starting point is the attractive interaction corresponding to the $\pi\pi$ system where $I = 0$ (isospin factor $f = -3$) which gives rise to the bound state (dot).

is taken to be exactly the same as for the $\pi\pi$ case (projected now onto isospin $I = 1$). However, as can be seen from Tables I and IV, the important $\rho$ exchange between two kaons becomes repulsive for isospin $I$=1, destroying the $K\overline{K}$ bound state we found for $I$=0. To illustrate this we considered only the direct $K\overline{K}$ interaction and gradually changed the isospin factor for $\rho$ exchange from $-3$ to 1. Figure 12 shows the motion of the bound state pole that results. As the $K\overline{K}$ interaction decreases the bound-state pole on the $[bt]$ (=$[tt]$) sheet crosses the $K\overline{K}$ threshold to the $[t\dot{b}]$ (=$[b\dot{b}]$) sheet and moves down along the real axis to energies far away from $K\overline{K}$ threshold.

Although the preceding remarks rule out a $K\overline{K}$ bound-state (or anti-bound-state) structure for the $a_0$ our consistent meson exchange framework allows us to proceeded anyway to construct a model for $\pi\eta$ scattering as described in Sec. II. As already noted, only one additional parameter is needed, namely, the cutoff mass $\Lambda_{\eta KK^*}$. Before we discuss our results some remarks should be made concerning the available experimental information which, in contrast with the $\pi\pi$ interaction, is rather poor for the $\pi\eta$ case. The parameters of the $a_0$ have been derived indirectly from the mass spectra of relatively complicated processes such as $pp \to pp\eta\pi^+\pi^-$ [13] and recent values obtained from conventional Breit-Wigner fits are, e.g.,

$$m_{a_0} = (982 \pm 2)\ \text{MeV},\ \Gamma_{a_0} = (54 \pm 10)\ \text{MeV}\ [21],$$

$$m_{a_0} = (984 \pm 4)\ \text{MeV},\ \Gamma_{a_0} = (95 \pm 14)\ \text{MeV}\ [22]. \quad (13)$$

We note that there would still appear to be some uncertainty concerning the width of the $a_0$. Interestingly, the Particle Data Group, in its latest work [13], chose not to calculate an averaged width for the $a_0$ (as well as for the $f_0$). Their values are

$$m_{a_0} = (982.4 \pm 1.4)\ \text{MeV},\ \Gamma_{a_0} = 50 - 300\ \text{MeV}. \quad (14)$$

The reason is that the values derived from experimental results [see, e.g., Eq. (13)] give only the peak width while the decay width may be much larger. We concur with this opinion. As we will see, our results suggest a very broad $a_0$ if the width is correctly determined from the pole position.

Figure 13(a) shows the sensitivity of our calculation for the $\pi\eta$ cross section on the only remaining relevant parameter not constrained by the $\pi\pi$ system, namely, the cutoff mass $\Lambda_{\eta KK^*}$.

Although the shape of the cross section depends on the parameter choice we always observe a peak around the $K\overline{K}$ threshold. Looking at the pole structure of the corresponding $\pi\eta$ $T$ matrix a single pole on the $[bt]$ sheet is found for each value of $\Lambda_{\eta KK^*}$ [Fig. 13(b)]. For a pole position below $K\overline{K}$ threshold the corresponding cross sections have a rounded peak form whereas for values above (where a $[bb]$ pole at the same position would be closer to the physical region) we observe a cusp structure.

In order to get a feeling for the origin of the observed $[bt]$ pole we have excluded the direct $K\overline{K}$ interaction in Fig. 14. Although the pole is now always found above $K\overline{K}$ threshold, it is still present. We therefore conclude it must originate from the transition potential $\pi\eta \to K\overline{K}$ and hence is a dynamically generated effect of the opening of the $K\overline{K}$ channel. However, the direct $K\overline{K}$ interaction appears to be an important contribution in order to obtain reasonable agreement with experimental information. It is obvious that the cusplike cross sections of Fig. 14(a) do not yield $a_0$ parameters in agreement with the Breit-Wigner fits summarized in Eq. (13).

Compared to $K^*$ exchange in the $\pi\pi \to K\overline{K}$ transi-

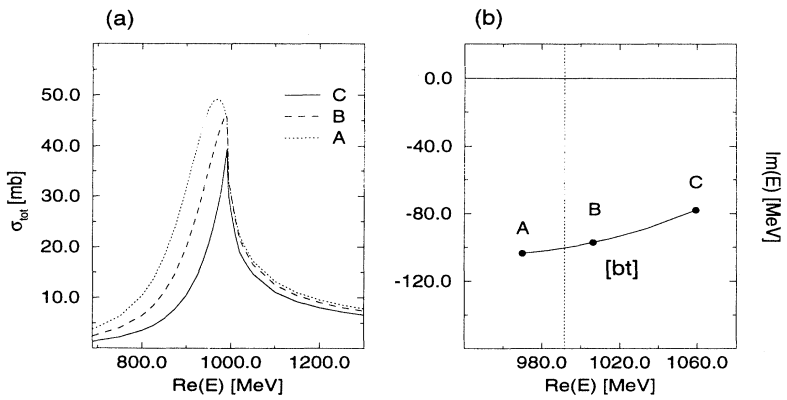


FIG. 13. The $\pi\eta$ cross section (a) and the corresponding pole position (b) for different choices of the parameter $\Lambda_{\eta KK^*}$. $A$, 3.6 GeV; $B$, 3.1 GeV; $C$ 2.6 GeV.

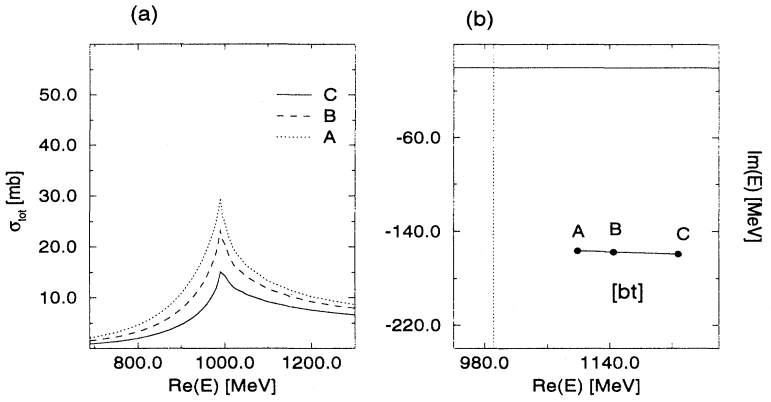


FIG. 14. The same as Fig. 13 but without any direct $K\overline{K}$ interaction. The values of $\Lambda_{\eta KK^*}$ are $A$, 5.0 GeV; $B$, 4.0 GeV; $C$, 3.1 GeV.

tion potential, the corresponding diagram for $\pi\eta \to K\overline{K}$ appears to be stronger. This can already be seen by calculating the factor $C$ of Eq. (A4) for $K^*$ exchange yielding $C(\pi\eta \to K\overline{K}) = \sqrt{2}C(\pi\pi \to K\overline{K})$. In addition, the total $\pi\pi/K\overline{K}$ transition potential is reduced by a partial cancellation between $K^*$ $t$-channel and $\epsilon$ $s$-channel exchange. Figure 15 demonstrates the crucial role of the $\pi\eta \to K\overline{K}$ coupling strength for the $a_0$ structure. When this coupling is decreased only slightly the $[bt]$ pole moves to an energy region where it no longer has any effect on physical observables.

Figure 16 shows the cross section for our full model with $\Lambda_{\eta KK^*}$ adjusted so that a Breit-Wigner fit to our calculated cross section roughly agrees with that obtained by fits to the available data. The mass and width of the $a_0$ determined from this cross section are $m_{a_0} \simeq 985$ MeV and $\Gamma_{a_0} \simeq 110$ MeV, in reasonable agreement with the experimental values of Ref. [22] while the lower values of, e.g., Ref. [21] cannot be obtained within our model. The "real" values for the $a_0$ parameters, however, can only be obtained from the position of the pole and so we finally find, in our model,

$$m_{a_0} = 991 \text{ MeV}, \qquad \Gamma_{a_0} = 202 \text{ MeV}. \tag{15}$$

The $a_0$ width determined from our pole analysis turns out to be much larger than the standard values [Eq. (13)]. The observed narrower peak in the cross section is a consequence of the closeness to the $K\overline{K}$ threshold. This is in agreement with other investigations [23,24] which also find that the $a_0$ is not really narrow and concurs with the recent statements of the Particle Data Group.

## IV. CONCLUSIONS

In summary, we have investigated the structure of the scalar mesons $f_0(980)$ and $a_0(980)$ in the framework of a meson exchange model for $\pi\pi$ and $\pi\eta$ scattering. The latter has been obtained by a consistent extension of the

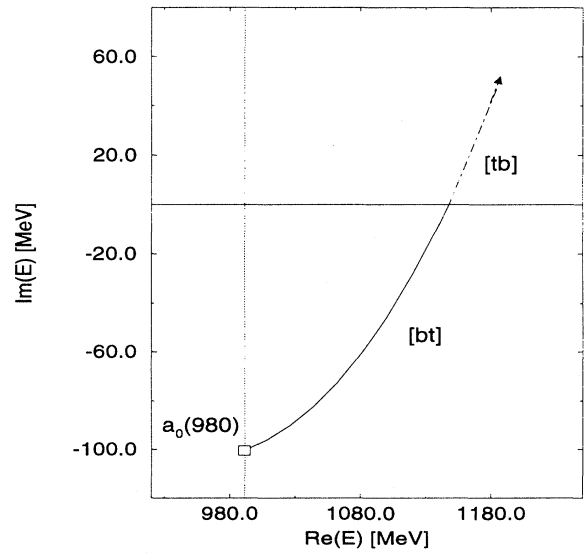


FIG. 15. The movement of the $a_0(980)$ pole as the $\pi\eta/K\overline{K}$ coupling strength is decreased. When the pole crosses the real axis the reduction factor is about 0.8.

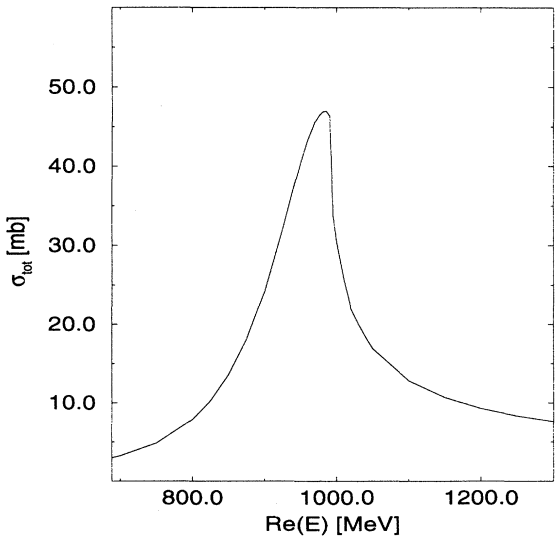


FIG. 16. The $\pi\eta$ cross section for our full model.

TABLE V. A summary of all poles found in the $\pi\pi - K\overline{K} - \pi\eta$ system.

| $I$ | $J$ | Sheet | Pole position [MeV] | Comment |
|---|---|---|---|---|
| 0 | 0 | $[bt]$ (II) | $(387, \pm 305)$ | $\sigma(400)$ |
| 0 | 0 | $[bb]$ (III) | $(314, \pm 428)$ | $\sigma(400)$ shadow pole |
| 0 | 0 | $[bt]$ (II) | $(1015, \pm 15)$ | $f_0(980)$ |
| 0 | 0 | $[bb]$ (III) | $(1346, \pm 249)$ | effective $f_0(1400) - f_0(1590)$ |
| 1 | 1 | $[bt]$ (II) | $(775, \pm 82)$ | $\rho$ |
| 1 | 0 | $[bt]$ (II) | $(991, \pm 101)$ | $a_0(980)$ |

Jülich model for the $\pi\pi$ interaction [9].

Our solution for the $\pi\pi$ scattering amplitude is shown to be compatible with the available experimental data sets. In particular, we are able to describe data on $J/\psi \to \phi\pi\pi/\phi K\overline{K}$ decay which has been considered to be an important testing criterion for models of the $f_0(980)$. By exploring the pole positions of the $\pi\pi$ $T$ matrix (see Table V) we found the $f_0(980)$ to be a narrow $K\overline{K}$ bound state of relatively large mass ($m_{f_0} = 1015$ MeV). We also found a very broad $\sigma(400)$ pole on the $[bt]$ sheet (cf. Ref. [10]) which generates the large $\pi\pi$ $S$-wave phase shifts below 1.0 GeV. For high energies, the pole of a heavy scalar particle with $q\bar{q}$ structure is observed on the $[bb]$ sheet which is interpreted as a mixture of two scalar mesons, such as $f_0(1400)$ and $f_0(1590)$.

A consistent extension of our model to the $\pi\eta$ channel generates a pole on the $[bt]$ sheet relatively close to $K\overline{K}$ threshold. Looking at the corresponding $\pi\eta$ cross section we find a peak structure in reasonable agreement with the experimental information available for the parameters of the $a_0(980)$. However, the mass and width derived from the pole position show the $a_0(980)$ to be rather broad. We discussed the role of the direct $K\overline{K}$ interaction for our results and found it to be not essential for the generation of a pole though it improves the agreement with experimental data. The origin of the $[bt]$ pole assigned to the $a_0(980)$ is therefore the transition potential $\pi\eta \to K\overline{K}$.

In conclusion, both scalar mesons, $f_0(980)$ and $a_0(980)$, result from the coupling to the $K\overline{K}$ channel which explains in a natural way their similar properties. The underlying structure, however, is quite different. Whereas the $f_0(980)$ appears to be a $K\overline{K}$ bound state the $a_0(980)$ is found to be a dynamically generated threshold effect. To finally decide about the parameters of these mesons additional experimental information on $K\overline{K}$ production and the $\pi\eta$ system is required. A corresponding experiment is, for example, proposed for the Jülich proton synchrotron COSY [25].

## ACKNOWLEDGMENTS

This work was supported in part by Deutscher Akademischer Austauschdienst (zweites Hochschulsonderprogramm) and the Australian Research Council. G. J. thanks G. E. Brown for the hospitality he enjoyed in Stony Brook and for many useful discussions.

## APPENDIX: POTENTIAL EXPRESSIONS

In this appendix we give explicit expressions for the potential describing the interaction between two pseudoscalar mesons of mass $m_p$. Some of them have already been derived in [9]. We write $V_{s/t} \equiv V_{s/t}(k_3, k_4; k_1, k_2; E)$ where $k_1$–$k_4$ are the four-momenta of the external mesons and the subscript denotes an $s$- or $t$-channel exchange. We have the following.

For scalar-meson exchange,

$$\mathcal{L}_{pps} = \frac{g_{pps}}{m_p}\partial^\mu\phi_p\partial_\mu\phi_p\phi_s,$$
$$V_t = \frac{4C}{m_p^2}\frac{k_{1\mu}k_3^\mu k_{2\nu}k_4^\nu}{t - M^2},$$
$$V_s = \frac{4C}{m_p^2}\frac{k_{1\mu}k_2^\mu k_{3\nu}k_4^\nu}{s - M_0^2}. \tag{A1}$$

For vector-meson exchange,

$$\mathcal{L}_{ppv} = g_{ppv}\phi_p\partial_\mu\phi_p\phi_v^\mu,$$
$$V_t = C\sum_\lambda \frac{(k_1 + k_3)^\mu(k_2 + k_4)^\nu\epsilon_\mu^*\epsilon_\nu}{t - M^2},$$
$$V_s = C\sum_\lambda \frac{(k_1 - k_2)^\mu(k_3 - k_4)^\nu\epsilon_\mu^*\epsilon_\nu}{s - M_0^2}. \tag{A2}$$

For tensor-meson exchange,

$$\mathcal{L}_{ppt} = \frac{g_{ppt}}{m_p}\partial^\mu\phi_p\partial^\nu\phi_p\phi_{t\mu\nu},$$
$$V_t = \frac{C}{m_p^2}\sum_\lambda(k_{1\mu}k_{3\nu} + k_{3\mu}k_{1\nu})(k_{2\sigma}k_{4\tau} + k_{4\sigma}k_{2\tau}) \times\frac{\epsilon^{*\mu\nu}\epsilon^{\sigma\tau}}{t - M^2},$$
$$V_s = \frac{C}{m_p^2}\sum_\lambda(k_{1\mu}k_{2\nu} + k_{2\mu}k_{1\nu})(k_{3\sigma}k_{4\tau} + k_{4\sigma}k_{3\tau}) \times\frac{\epsilon^{*\mu\nu}\epsilon^{\sigma\tau}}{s - M_0^2}. \tag{A3}$$

Here, $\epsilon^\mu$ denotes the polarization vector of an exchanged vector meson, which depends on the exchanged momentum and helicity $\lambda$, while $\epsilon^{\mu\nu}$ is the corresponding object for exchanged tensor mesons. The mass of the exchanged particle is denoted by $M$. For $s$-channel processes the multiple scattering series renormalizes the exchanged meson so a bare mass $M_0$ is used, which in each case is adjusted to fit an observed resonance.

The $u$-channel contributions can be obtained by exchanging $k_3$ and $k_4$ and replacing $t$ by $u$.

The overall factor $C$ is given by

$$C = g^2 f n F^2. \tag{A4}$$

Here, $F$ denotes a standard form factor of dipole type

$$t,\ u \text{ channel:} \qquad F = \left(\frac{2\Lambda^2 - M^2}{2\Lambda^2 - (\mathbf{k}' \mp \mathbf{k})^2}\right)^2;$$

$$s \text{ channel:} \qquad F = \left( \frac{2\Lambda^2 - k_0^2(M)}{2\Lambda^2 - |\mathbf{k}|^2} \right)^2 . \qquad \text{(A5)}$$

Here $\mathbf{k}$ and $\mathbf{k}'$ denote the initial and final c.m. momenta and $k_0(E)$ is the on-shell momentum defined in Eq. (3). [For $s$-channel contributions, the $F^2$ appearing in Eq. (A4) is really $F(\mathbf{k})F(\mathbf{k}')$.] The corresponding cutoff masses $\Lambda$, together with coupling constants $g^2/4\pi$, isospin factors $f$, and bare masses $M_0$, are given in Tables I–IV. The isospin factors $f$ are derived from the standard isospin structure of the Lagrangians, which was suppressed in Eqs. (A1)–(A3). The factor $n$ takes into account the normalization of states for identical particles [9]. It is $1/2$ for $\pi\pi \to \pi\pi$, $1/\sqrt{2}$ for $\pi\pi \to K\overline{K}$ and 1 for $K\overline{K} \to K\overline{K}$, $\pi\eta \to \pi\eta$ and $\pi\eta \to K\overline{K}$.

To evaluate the potentials explicitly the BS off-shell prescription has to be applied for the different momenta:

$$k_1 = \left( \frac{\sqrt{s}}{2} + c, \mathbf{k} \right), \qquad k_2 = \left( \frac{\sqrt{s}}{2} - c, -\mathbf{k} \right), \qquad \text{(A6)}$$

and

$$k_3 = \left( \frac{\sqrt{s}}{2} + c', \mathbf{k}' \right), \qquad k_4 = \left( \frac{\sqrt{s}}{2} - c', -\mathbf{k}' \right), \qquad \text{(A7)}$$

where

$$c, c' = \begin{cases} \frac{m_\pi^2 - m_\eta^2}{2\sqrt{s}} & \text{for } \pi\eta \,, \\ 0 & \text{for } \pi\pi,\ K\overline{K}. \end{cases} \qquad \text{(A8)}$$

Finally, a standard partial wave expansion is performed to obtain potentials suitable for use in Eq. (1).


[1] D. Morgan, Phys. Lett. **51B**, 71 (1974).
[2] J. Weinstein and N. Isgur, Phys. Rev. D **41**, 2236 (1990).
[3] R. L. Jaffe, Phys. Rev. D **15**, 267 (1977).
[4] D. Morgan and M. R. Pennington, Phys. Rev. D **48**, 1185 (1993).
[5] D. Morgan and M. R. Pennington, Phys. Rev. D **48**, 5422 (1993).
[6] A. Falvard *et al.*, Phys. Rev. D **38**, 2706 (1988).
[7] W. Lockman, in *Hadron '89, Proceedings of the 3rd International Conference on Hadron Spectroscopy*, Ajaccio, France, edited by F. Binon *et al.* (Editions Frontières, Gif-sur-Yvette, 1989).
[8] B. C. Pearce and B. F. Gibson, Phys. Rev. C **40**, 902 (1989).
[9] D. Lohse, J. W. Durso, K. Holinde, and J. Speth, Nucl. Phys. **A516**, 513 (1990).
[10] B. S. Zou and D. V. Bugg, Phys. Rev. D **50**, 591 (1994).
[11] D. Morgan and M. R. Pennington (unpublished); and (private communication).
[12] B. S. Zou and D. V. Bugg, Phys. Rev. D **48**, R3948 (1993).
[13] Particle Data Group, L. Montanet *et al.*, Phys. Rev. D **50**, 1173 (1994), p. 1465.
[14] B. C. Pearce, K. Holinde, J. Speth, and R. Tegen, Few Body Sys. Suppl. **6**, 50 (1992).
[15] R. Blankenbecler and R. Sugar, Phys. Rev. **142**, 1051 (1966).
[16] B. C. Pearce and I. R. Afnan, Phys. Rev. C **30**, 2022 (1984).
[17] S. J. Lindenbaum and R. S. Longacre, Phys. Lett. B **274**, 492 (1992).
[18] A. D. Martin and E. N. Ozmutlu, Nucl. Phys. **B158**, 520 (1979).
[19] D. Cohen, D. S. Ayres, R. Diebold, S. L. Kramer, A. J. Pawlicki, and A. B. Wicklung, Phys. Rev. D **22**, 2595 (1980).
[20] C. D. Frogatt and J. L. Petersen, Nucl. Phys. **B129**, 89 (1977).
[21] A. Amsler *et al.*, Phys. Lett. B **291**, 347 (1992).
[22] A. Armstrong *et al.*, Z. Phys. C **52**, 389 (1991).
[23] S. Flatté, Phys. Lett. **63B**, 224 (1976).
[24] N. N. Achasov, S. A. Devyanin, and G. N. Shestakov, Phys. Lett. **96B**, 168 (1980).
[25] *Proceedings of Workshop on Mesons and Mesonic States up to Slightly Above 1 GeV/$c^2$*, edited by W. Oelert and T. Sefzick (KFA, Jülich, 1991).
[26] B. R. Martin, D. Morgan, and G. Shaw, *Pion-pion Interactions in Particle Physics* (Academic, London, 1976).
[27] W. Ochs, Ph.D. thesis, Universität München, 1973.